ESTIMATING STRUCTURAL INTEGRITY OF TYPE 304 STAINLESS STEEL PLATES AND PIPES CONTAINING SMALL DEFECTS

W. G. REUTER, F. W. SMITH

EG & G Idaho, Inc., Fuels and Materials Division, P.O. Box 1625, Idaho Falls, Idaho 83401, U.S.A.

T. A. PLACE

Mechanical Engineering Department, University of Idaho, Moscow, Idaho 83843, U.S.A.

SUMMARY

In recent years there has been considerable demand for accurate assessment of the influence of defects on structural component integrity. Analyses used must account for the effect of large plastic deformation of low-strength ductile materials. A number of models have been developed for the analysis of reactor coolant piping as well as less ductile plate and piping, but these models have not been verified for the full spectrum of potential materials and configurations encountered in reactor components. This paper presents preliminary test program results and some evaluation of these models, specifically the flow stress approach and the two-parameter fracture criterion (TPFC). The tests were conducted with annealed Type 304 stainless steel flat tensile specimens containing triangular, rectangular, or part-circular surface flaws, and pressurized pipe specimens with internal or external triangular surface defects.

The flow stress approach was found to be unsatisfactory as indicated by the conservative estimate for the pipe specimen and by the large amount of scatter for the flat plate specimens. The TPFC approach was used in conjunction with the initial defect size and the loads required for crack initiation as well as the load at penetration. There is a tendency for the TPFC to overpredict crack initiation stress intensity for small cracks and underpredict initiation stress intensity for large cracks, but there appears to be no effect of the defect configuration. The TPFC predicts penetration stress intensity more closely over the full range of crack size and in this case there is a definite dependence on defect configuration with the rectangular flaws having lower stress intensity than the others. Even though some modification may be necessary, the TPFC approach may have broad applicability since the data for the pipe specimens are in reasonable agreement with the data for the flat plate specimens.

1. Introduction

In recent years there has been considerable demand for accurate assessment of the influence of defects on structural component integrity in both experimental and commercial nuclear reactors. The analyses used must account for the effects of large plastic deformation of the low-strength ductile materials used in reactor construction.

A number of models have been developed by Maxey et al [1], Kiefner et al [2] and Vandenburg and Imhoff [3] for the analysis of reactor coolant piping and by Newman [4, 5] for less ductile plate and piping. The available models, however, have not been verified for the full spectrum of potential materials and configurations for reactor components, and in some instances have been found to be deficient. Thus they are subject to question when used to analyze problems involving materials and configurations for which they have not been verified.

In order to improve the data base against which models may be tested and to gain information about the behavior of Type 304 stainless steel (SS) in the presence of defects, a test program was conducted using surface-flawed plate specimens and pressurized pipe specimens with internal and external surface defects. This paper presents preliminary results from the test program, and some evaluation of the models presented in References 2, 4, and 5.

2. Test Program

2.1 Test Specimens

The chemistry and tensile properties for the annealed Type 304 SS flat plate and pipe material used in the test program are shown in Table I. Test specimens were fabricated from 13-mm (0.5-in.) thick flat plate and 15.9-mm (0.63-in.) wall, 152.4-mm (6-in.) diameter pipe. The gage section of the flat plate specimens was 6.35-mm (0.25-in.) thick by 177.8-mm (7.0-in.) wide by 355.6-mm (14.0-in.) long. The gage section of the pipe was 6.35-mm (0.25-in.) thick by 167.64-mm (6.6-in.) OD with a length of 101.6-mm (4.0-in.) plus the length (2c) of the surface defect. Surface defects were electric-discharge machined (EDM) in the centers of the gage length for both the flat plate and pipe specimens. The EDM defects had a maximum included angle of 30° and radius of 0.102-mm (0.004-in.), a nominal width of 0.305 mm (0.012 in.), and a depth (a) of 1.78, 3.56, or 5.08 mm (0.070, 0.140, or 0.200 in.). These depths represent 28%, 56%, and 80% of the thickness in the gage section. The aspect ratios (a/2c) were 0.1 or 0.5. Surface defects of rectangular, triangular, or part-circular configuration were located with the 2c dimension transverse to the 355.6-mm (14.0-in.) long gage section of the flat plates. The plate specimens were tested in straight rising load to instability or to the 127-mm (5-in.) stroke limitation of the test machine. Surface defects of triangular configuration were located on the ID or OD and oriented so that the 2c direction was parallel to the axial direction of the pipe. The pipe specimens were pressurized until the defect penetrated.

2.3 Data

The data collected consisted of: (1) load vs pinhole displacement, to allow estimation of the energy supplied to the specimen; (2) strain vs load, to determine the nominal strain at initiation and instability, as well as the extent of strain perturbation due to the crack; (3) crack-opening displacement (COD) vs load, to identify instability and to establish possible correlations with the defect configuration; (4) acoustic emission vs load, to determine the load corresponding to initiation of subcritical crack growth. Test conditions were established and documented in several ways: motion pictures, still photographs, and visual observations were made to enhance the understanding of the crack initiation and growth process; uniformity of loading and extent of the perturbation due to the defect were established using a photoelastic coating; and the load corresponding to defect penetration was determined from visual observations and by using an air bulb device attached to the back of some of the flat plate specimens.

3. Typical Data

3.1 Load Versus Displacement

Examples of typical load-vs-displacement plots for plate specimens are shown in Figure 1. The loads for instability ranged from 0.311 to 0.609 MN (70 to 137 kip), compared to the loads corresponding to yield and ultimate tensile strength, which are 0.311 and 0.712 MN (70 and 160 kip) respectively. Without question, the tests were conducted well into the plastic region. The curves in Figure 1 correspond to different crack sizes, the specimens containing larger initial defects reaching instability at the lower loads.

3.2 Strain Gages and Reflective Photoelastic Coatings

The strain gage data showed that no bending occurred during the tests. The data from gages located 51 and 102 mm (2 and 4 in.) above the centerline of the crack showed good agreement with one another. This agreement was verified by the symmetry of the isochromatic fringes obtained from the reflective photoelastic coating, see Figure 2. Figure 2 shows that the defect has a considerable effect on the localized strain distribution. For a photoelastic coating thickness of 0.508 mm (0.022 in.), the approximate value of $\varepsilon_1-\varepsilon_2$ per fringe is 0.04. The data indicated that the defect had negligible effect on the nominal strain in the region extending 51 to 102 mm (2 to 4 in.) beyond the defect in the direction normal to the crack plane. In the crack plane the perturbation to the strain field was substantial, as shown by the photoelastic coatings, see Figure 2.

3.3 Attainment of Instability

The use of still and motion pictures in conjunction with visual observations, COD, acoustic emission measurements, and the air bulb device allowed for partial explanation of the process leading to attainment of instability. The sequence of events consists of the following: (1) substantial blunting of the crack tip, which may overwhelm the effects of the initial crack tip sharpness; (2) work hardening of the plastic zone to the extent indicated in Figure 3; (3) initiation of subcritical crack growth, detected by acoustic emission monitoring; (4) subcritical crack growth, detected by acoustic emission, COD, and various optical observations; and (5) attainment of instability, which in many instances coincides with penetration of the defect through the wall thickness. Penetration was indicated by the horizontal slope of the COD-vs-load plot and detected by the air bulb device which began filling at penetration because air leaked through the crack.

The load-displacement plot shown in Figure 1 for specimen 12 indicates it was loaded to 0.480 MN (108 kip) which corresponds to 425.8 MPa (61.7 ksi) or about 7% nominal strain. Specimen 28 was one of the few specimens where the test was terminated upon the defect penetrating the wall thickness. This occurred at 0.311 MN (70 kip), which corresponds to 276 MPa (40 ksi) or about 0.4% strain. The purpose of Figure 3 is to identify that significant work hardening had occurred in the vicinity of the crack. These results are only for identification of trends since the hardness traverses were not taken from the crack tip but were offset slightly because the specimen had been separated by an abrasive cut-off wheel.

4. Analysis of Results

4.1 Flat Plate Specimens

4.1.1 Approach Developed by Kiefner et al [2]

This approach was used for the flat plate specimens by assuming that the flat plate was a pipe of infinite radius. From Reference 2

$$\frac{\sigma_f}{\bar{\sigma}} = \frac{1-\frac{a}{t}}{1-\frac{a}{M_T t}} \tag{1}$$

where σ_f = failure stress

$\bar{\sigma}$ = flow stress   a = depth of flaw

M_T = Folias correction factor   t = pipe wall thickness

The factor M_T is taken to be unity for flat plate specimens. Substituting M_T = 1.0 results in $\sigma_f = \bar{\sigma}$, that is, failure stress equals flow stress. The flow stress was calculated for the load corresponding to defect penetration and the results are summarized in Table II. From Table II it may be shown that the ratio of $\bar{\sigma}_{test}$ to $\bar{\sigma}_{calc}$ varies from 0.62 to more than 1.33. The simple theory which results from taking eq. (1) to its limit proves to be quite inadequate.

4.1.2 Two-Parameter Fracture Criterion (TPFC)

Newman [4, 5] has developed a two-parameter model for fracture under conditions dominated by plastic deformation. The criterion for fracture is expressed in the form

$$K_{Ie} = \sqrt{\pi c F^2}\ \left[\sqrt{(m\gamma)^2 + 2\gamma\sigma_{ult}} - m\gamma\right] \tag{2}$$

where

$$\gamma = \sigma_{ys} K_f / (2\sigma_{ult} \sqrt{\pi c F^2}) \tag{3}$$

In eqs. (2) and (3), K_f and m are the two fracture parameters which are independent of crack size and shape. K_f, however, is dependent upon specimen thickness. The factor F, found in Reference 5, is an elastic magnification factor for semielliptical surface cracks.

This fracture criterion is intended to predict the peak load during a rising-load-to- failure experiment. In the present work an attempt has been made to apply this criterion to predicting both the condition of crack initiation as sensed by acoustic emission and the condition for the crack penetrating the wall thickness.

The initial defect size, the loads required for initiation of subcritical crack growth, and the load at penetration were used to calculate K_{Ie} and cF^2, see Figure 4. Figure 4 was developed using the equation for an ellipse regardless of the actual crack configuration. The lower two solid lines in Figure 4 are the predictions for initiation of subcritical crack growth based on eqs. (2) and (3) for m equal to unity and values of K_f as noted. The data follow the general shape of the fracture criterion; however, there is a tendency for the criterion to overpredict at low cF^2 values and underpredict at high cF^2 values. There appears to be no effect of the defect configuration, as indicated by the random distribution of data for all three configurations. There appears to be a definite dependence on defect configuration for penetration, as shown by the data for the rectangular defect lying near the curve for K_f = 209 MPa·m$^{1/2}$ (190 ksi·in.$^{1/2}$) and m = 1.0, whereas data for the elliptical and triangular defects are scattered near a curve corresponding to K_f = 330 MPa·m$^{1/2}$ (300 ksi·in.$^{1/2}$) and m = 1.0. The data are insufficient to ascertain, with any degree of certainty, whether the specimens containing triangular defects behave differently from those containing part-circular defects.

4.2 Pipe Specimens

4.2.1 Approach Developed by Kiefner et al [2]

For the two pipe specimens with 167.6-mm (6.6-in.) OD, 6.27-mm (0.247-in.) wall thickness and the axially oriented surface defects located on either OD or ID, the flow stress was calculated on the basis of eq. (1). The results are summarized in Table III and it is apparent that $\bar{\sigma}_{test}$ is 1.22 to 1.27 times $\bar{\sigma}_{calc}$. This means that eq. (1) would provide a conservative estimate of the load required for penetration if the approach suggested in Reference 2 is used in conjunction with $\bar{\sigma}_{calc} = (\sigma_{ys} + \sigma_{uts})/2$. However, $\bar{\sigma}_{test}$ is limited to σ_{uts} which corresponds to 1.38 $\bar{\sigma}$.

4.2.2 Two-Parameter Fracture Criterion

The TPFC [4,5] was used to analyze the data for the pipe specimens. Since a problem was encountered with the acoustic emission monitoring system used to detect the load corresponding to initiation of subcritical crack growth, only the data for penetration were used. Using the pipe specimen gage length of 107.2 mm (4.22 in.) in place of the plate width, K_{Ie} and cF^2 were calculated to be 51.8 MPa·m$^{1/2}$ (47.1 ksi·in.$^{1/2}$) and 2.54 mm (0.100 in.) for specimen C and 44.2 MPa·m$^{1/2}$ (40.2 ksi·in.$^{1/2}$) and 2.03 mm (0.080 in.) for specimen M. These points are plotted in Figure 4 and there is reasonable agreement with the values from the flat plate specimens.

5. Conclusions

When only pressure loadings are imposed, the approach developed by Kiefner et al [2] has been effective for predicting the behavior of pipe material of the same general configuration as that used to develop the empirical correlations. The approach is not, however, accurate for predicting the behavior for different configurations. This is apparent from the contrast between estimates for the plate and pipe specimens. The estimate of the stress required for the defect in the pipe specimen to penetrate the wall thickness is conservative. The predicted stresses for the flat plate specimens, assumed to be pipes of very large diameter, are not always conservative since they vary from 0.62 to >1.33 that of the actual stress for failure.

It is evident that the TPFC is more flexible than the approach developed by Kiefner et al [2], since it may be used to predict the behavior for both elastic conditions [4,5] and the plastic conditions encountered in this test program. Additional work is needed to modify K_f and m in order to conform with the test data as shown in Figure 4. The TPFC also has some promise of being applicable to pipes as well as to flat plates. For design purposes it would be possible to analyze the effects of a defect on structural integrity using either the load corresponding to initiation of subcritical crack growth or the load required for the defect to penetrate the wall thickness.

References

/1/ MAXEY, W. A., KIEFNER, J. F., EIBER, R. J., and DUFFY, A. R., "Ductile Fracture Initiation, Propagation and Arrest in Cylindrical Vessels", Fracture Toughness, Proceedings of the 1971 National Symposium on Fracture Mechanics, Part II, ASTM STP 514, American Society for Testing and Materials, pp 70-81 (1972).

/2/ KIEFNER, J. F., MAXEY, W. A., EIBER, R. J., and DUFFY, A. R., "Failure Stress Levels of Flaws in Pressurized Cylinders", Progress in Flaw Growth and Fracture Toughness Testing, ASTM STP 536, American Society for Testing and Materials, pp 461-481 (1973).

/3/ VANDENBURG, S. R., IMHOFF, D. H., Reactor Primary Coolant System Rupture Study, GEAP-5637, General Electric Company APED (June 1968).

/4/ NEWMAN, J. C., Jr., "Fracture Analysis of Various Cracked Configurations in Sheet and Plate Materials", Properties Related to Fracture Toughness, ASTM STP 605, American Society for Testing and Materials, pp 104-123 (1976).

/5/ NEWMAN, J. C., JR., "Fracture Analysis of Surface- and Through-Cracked Sheets and Plates," Engineering Fracture Mechanics, 5, pp 667-689 (1973).

TABLE I

ROOM TEMPERATURE MECHANICAL PROPERTIES AND CHEMISTRY
FOR THE TYPE 304 STAINLESS STEEL USED IN TEST PROGRAM

Material Identification	σ_{ys}		σ_{uts}		%El	%RA	Cr	Ni	Mn	C	Si	Mo	P	S	Fe
	MPa	ksi	MPa	ksi											
Flat Plate -1	253	36.7	663	96.1	71.3	67.8	18.35	9.00	1.33	0.04	0.53	0.21	0.016	0.010	Bal
Flat Plate -2	260	37.6	603	87.5	70.6	76.4	18.75	9.60	1.70	0.06	0.49	0.48	0.020	0.019	Bal
Flat Plate -3	254	36.9	621	90.1	80.0	59.8	18.15	9.05	1.09	0.05	0.62	0.18	0.020	0.013	Bal
Pipe - Axial Orient. 4.02 mm (0.158 in.) dia.	257	37.3	601	87.2	67.3	67.7	18.85	9.65	1.52	0.060	0.52	0.24	0.029	0.013	Bal
6.33 mm (0.249 in.) dia.	253	36.6	603	87.4	75.5	75.2									
Pipe - Circum. Orient. 4.06 mm (0.160 in.) dia.	291	42.2	602	87.4	70.0	70.1									

TABLE II

COMPARISON OF EXPERIMENTALLY DETERMINED FAILURE STRESS WITH CALCULATED FLOW STRESS FOR TYPE 304 SS FLAT PLATE SPECIMENS

Identification	Range of $\bar{\sigma}_{test}$ for Penetration		$\bar{\sigma}_{calc}$, where $\bar{\sigma}_{calc} = \frac{\sigma_{ys} + \sigma_{uts}}{2}$	
	MPa	ksi	MPa	ksi
Plate I	295.3 to > 569.9	42.8 to > 82.6	429.2	62.2
Plate II	328.4 to > 538.9	47.6 to > 78.1	327.8	62.0

Note: $\bar{\sigma}_{test}$ is the flow stress calculated from eq. (1) using test data for failure stress.

TABLE III

COMPARISON OF EXPERIMENTALLY DETERMINED FLOW STRESS WITH CALCULATED FLOW STRESS FOR TYPE 304 SS PIPE SPECIMENS

Specimen Identification	Crack Depth (a)		Crack Length (2c)		$\frac{1-a/t}{1-a/M_T t}$	test	
	mm	in.	mm	in.		MPa	ksi
C (defect on ID)	1.98	0.078	18.0	0.71	0.977	567.9	82.3
M (defect on OD)	1.55	0.061	18.0	0.71	0.984	545.8	79.1

$\bar{\sigma}_{calc} = (\sigma_{ult} + \sigma_{ys})/2 = \frac{322 + 603}{2} = 462$ MPa (65.0 ksi)

Note: $\bar{\sigma}_{test}$ is the flow stress calculated from eq. (1) using test data for failure stress.

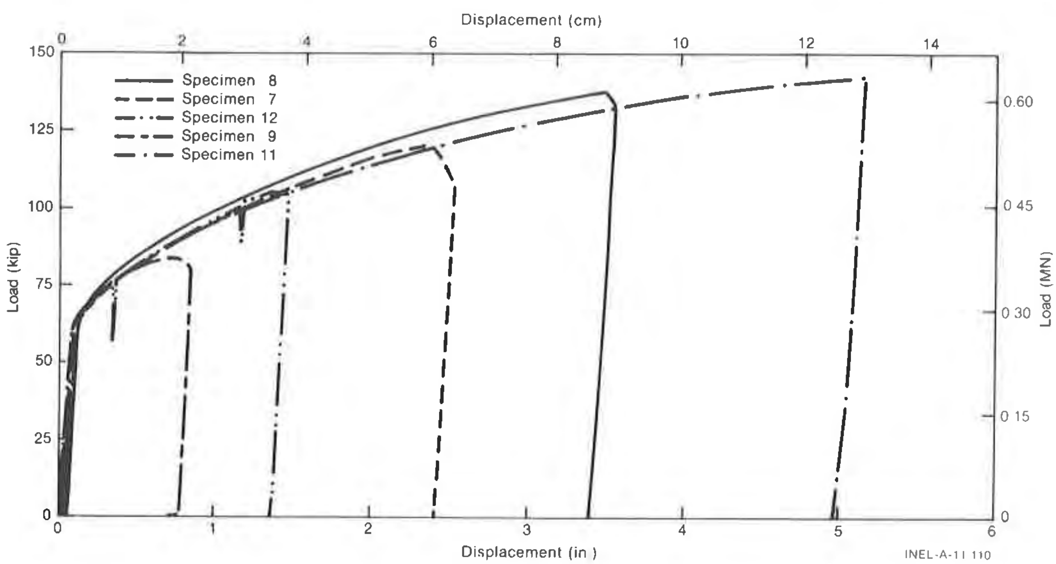

Fig. 1 Plot of load versus displacement for Type 304 stainless steel flat plate specimens.

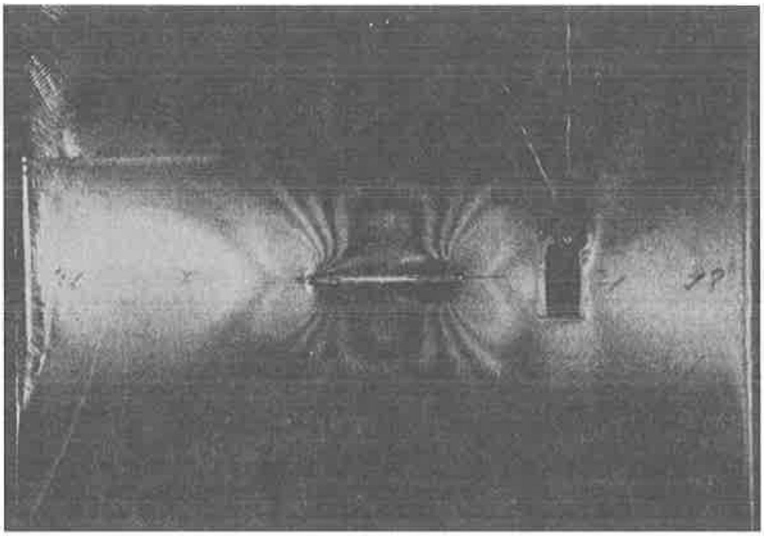

Fig. 2 Example of isochromatic fringe patterns from a reflective photoelastic coating mounted on a Type 304 stainless steel flat plate specimen.

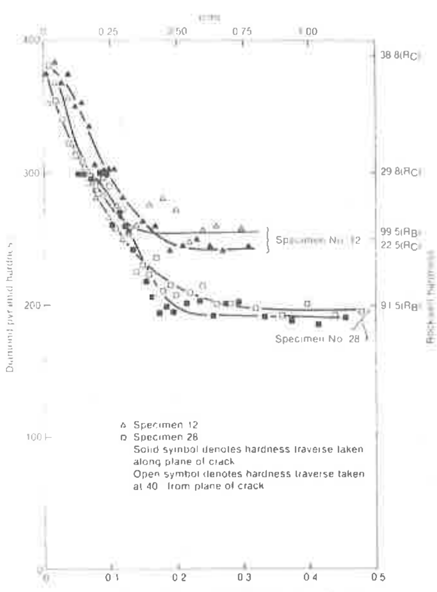

Fig. 3 Plot of hardness on the front surface versus distance from tip of the crack on a Type 304 stainless steel flat plate specimen.

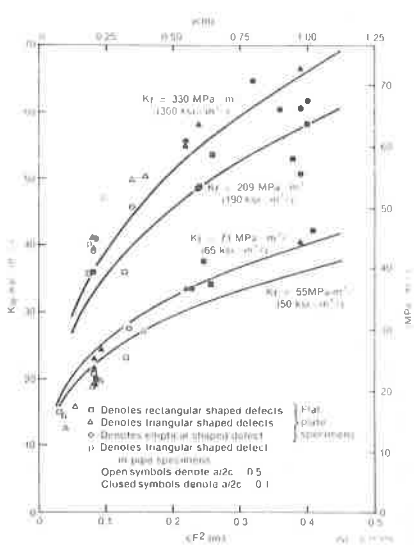

Fig. 4 Plot of K_{Ie} versus cF^2 for crack initiation and penetration in Type 304 stainless steel flat plate specimens.